A study of suffusion kinetics inspired from experimental data: comparison of three different approaches

A. Kodieh, Rachel Gelet, Didier Marot, A. Z. Fino

Noname manuscript No.
(will be inserted by the editor)

A study of suffusion kinetics inspired from experimental data: comparison of three different approaches

A. Kodieh · R. Gelet · D. Marot · A.Z. Fino

Received: date / Accepted: date

Abstract Suffusion is a complex phenomenon characterized by a selective migration of the fine particles under the effect of three coupled processes: detachment, transport and possible filtration of the fine fraction. With the objective to reproduce the kinetics of the suffusion process, a new energy-based constitutive relationship, inspired from the energy-based approach is proposed. Moreover, this energy-based relationship is compared with other constitutive relationships inspired from the shear stress-based approach and the power-based approach. Each predicted eroded mass evolution is consistently compared against experimental measurements. For each individual specimen, the shear stress-based constitutive relationship tackles well the initiation of the suffusion process but overestimates the development of the process. On the other hand, both the energy-based and the power-based constitutive relationships can reproduce reasonably well the evolution of the cumulative eroded mass. Finally, the intrinsic quality (i.e. independent of the sample size and of the loading path, at least at the laboratory scale) of all parameters is examined, advantages and drawbacks of each approach are also highlighted.

Keywords Internal erosion · Suffusion · Erodimeter · Energy-based approach · Erosion resistance index · Cumulative dissipated energy

1 Introduction

Hydraulic earth structures are threatened by two modes of failure, erosion and sliding. More than 96% of dam incidents are attributed to erosion [1] and

A. Kodieh
Institut GeM, UN-ECN-CNRS, Université de Nantes, 44600 Saint-Nazaire, France
E-mail: alaa.kodieh@univ-nantes.fr

R. Gelet
Institut GeM, UN-ECN-CNRS, Université de Nantes, 44600 Saint-Nazaire, France
E-mail: rachel.gelet@univ-nantes.fr

among these incidents, 46% are due to internal erosion. Internal erosion processes can concern either the soils which constitute the hydraulic structures or their foundations. The durability of hydraulic earth structures is challenged by the instabilities induced by both internal and external erosion processes. Yet, since settlements may be frequently monitored, the risk of overtopping in common usage is reduced and internal erosion may be viewed as the most uncertain hazard.

Internal erosion can arise at different locations in a structure, so that Fell and Fry [2] have distinguished four different processes: concentrated leak erosion, backward erosion, contact erosion and suffusion. This paper deals with suffusion, which takes place inside the soil matrix and selectively erodes the fine particles that move through the voids between the coarser particles. In literature several studies highlighted that suffusion is usually accompanied by self-filtration and clogging [3] [4] [5] [6] [7] [8]. In fact upon detachment, some of these detached particles can re-settle or be filtered in the bulk of the porous network, thus inducing local clogging [9]. As a sequel, this phenomenon can be accompanied by the increase of the *local* hydraulic gradient [10] [11] [12] and by the decrease of the hydraulic conductivity [3] [4] [13] [14]. Moreover, according to the type of hydraulic loading (i.e. tests performed under hydraulic gradient-controlled conditions or under flow rate-controlled conditions), the predominant process can either be filtration or erosion [15]. In consequence, suffusion is defined as the coupled process of detachment, transport of fine particles and possible filtration of some detached particles within the constrictions of the granular skeleton of the coarse fraction.

With the intent to assess the durability of hydraulic earth structures, seminal research on suffusion susceptibility was conducted as a first screening tool. Several geometric methods have been proposed solely based on the soil particle size distribution [16] [17], while some take into account the size distribution of the constrictions [18].

However, it is important to highlight that, even if the transport of particles is geometrically feasible, the action of hydraulic flow must be sufficient to detach the fine particles [19]. Up to date, there exist four distinct propositions to identify the relevant hydraulic loading [5]: the hydraulic gradient, the pore velocity, the hydraulic shear stress, and the power dissipated by flow. Since suffusion may induce a re-deposition or filtration of the fine particles provoking a clogging process, both the seepage velocity or the hydraulic conductivity, and the pressure gradient or the hydraulic gradient, should be taken into account to evaluate the hydraulic loading. Indeed, the hydraulic shear stress and the power dissipated by flow obey this condition. In the hydraulic shear stress-based constitutive relationship, Reddi et al. [3] have approximated the soil as uniform sized cylindrical capillary tubes, based on which the hydraulic shear stress is expressed as,

$$\tau = \frac{\gamma_w \Delta h}{\Delta L} \sqrt{\frac{8k_F}{n^F}} \tag{1}$$

where Δh is the hydraulic head drop between the inlet and the outlet sections, γ_w is the unit weight of water, ΔL is the distance between the two sections, k_F is the intrinsic permeability of the soil and n^F is its porosity. While the computation of the hydraulic shear stress needs an assumption on the soil water interface, Marot et al. [20] have proposed to model the hydraulic loading by the power expended by the flow,

$$P_{flow} = (\gamma_w \Delta z + \Delta P)Q \tag{2}$$

where Q is the fluid flow rate, Δz is the elevation between the inlet and the outlet sections and ΔP is the pressure drop between those sections. Since the history of the hydraulic loading appears as a key parameter in the suffusion development [8], the instantaneous flow power is integrated over time to obtain the instantaneous cumulative expended energy:

$$E_{flow}(t) = \int_{t_0}^{t} P_{flow}(t)dt \tag{3}$$

The end of the suffusion process is characterized by a constant permeability and a decreasing erosion rate which is herein referred to a final state and is denoted t_{max}. At the final state, experimental evidences have shown that the cumulative eroded mass m_{max} and the cumulative expended energy E_{max} were proportional in a repetitive manner [21],

$$I_\alpha = -\log\left(\frac{m_{max}}{E_{max}}\right) \tag{4}$$

where I_α is the erosion resistance index and $E_{max} = E_{flow}(t_{max})$. Based on this index, a gradual classification of the suffusion susceptibility is proposed from highly resistant to highly erodible. [21].

Now to describe the kinetics of the suffusion process, a relation is required between the hydraulic loading and the corresponding soil response in time. In literature, several constitutive relationships were proposed for various forms of internal erosion [22][23]; yet, very few attempts have been achieved for suffusion. Reddi et al. [3] expressed the rate of erosion by a hydraulic shear-based constitutive relationship, whereas Sibille et al. [24] proposed a power-based constitutive relationship. From the erosion resistance index, which is a material property, an energy-based constitutive relationship is proposed herein, under which the hydraulic loading is characterized by the cumulative expended energy and the corresponding erosion is characterized by the cumulative eroded mass. The predicted cumulative eroded mass is consistently compared against the cumulative eroded mass collected during suffusion tests performed by Le [25] and Zhong et al. [26]. Also, the soil's response obtained with proposed energy-based constitutive relationship is compared with the shear stress-based constitutive relationship, adapted from the works of Reddi et al. [3], and with

Table 1 Properties of tested gradations

Gradation	Properties						
	P (%)	G_r	C_u	$(H/F)_{min}$	$D(H/F)_{min}$ (mm)	Kenney and Lau's criterion	Chang and Zhang's criterion
4	0.21	2.29	7.06	0.600	0.490	Unstable	Stable
6	0.99	3.33	16.24	0.155	0.496	Unstable	Unstable

Note: P = percentage of particle smaller than 0.063mm; $G_r = d_{max}/d_{min}$ (d_{max} and d_{min}: maximal and minimal particle sizes characterizing the gap in the grading curve); C_u = uniformity coefficient; F and H are the mass percentages of the grains with a size lower than a given particle diameter d and between d and $4d$, respectively; $D(H/F)_{min}$ is the corresponding diameter with the minimum value of ratio H/F.

the power-based constitutive relationship proposed by Sibille et al. [24]. Finally, the intrinsic characteristic of the constitutive parameters are probed.

2 Experimental devices and test procedure

Two experimental devices designed to apply downward seepage flow were used during the experimental tests. The first is an erodimeter with a rigid wall cylindrical cell, named oedopermeameter (O) dedicated to coarse soils, under which several tests were performed and interpreted by Zhong et al. [26]. The second device is composed of a triaxial cell (T) dedicated to finer soil specimens, under which companion tests were performed and interpreted by Le [25]. The diameters of these devices are 280 mm and 50 mm respectively. With the objective to test specimens in the same oedometric conditions, the membrane of the triaxial erodimeter is surrounded by a steel mold. Details of each device are presented in [4] and [11], and general illustrations for these devices are presented in Figure 1.

Two cohesionless soils with a gap-graded distribution were selected (see Figure 2). Soil (4) is created by a mixture of Fontainebleau sand and gravel. Soil (6) is composed of mixtures of sand and gravel marketed by Sabliére Palvadeau in France. According to the particle size distribution based criterion proposed by Kenney and Lau [17], these soils are potentially unstable (see Table 1). As the gap ratio G_r is smaller than 3 for Soil 4, this soil is classified as internally stable by Chang and Zhang's [16] method. In both devices, the sample is supported by a lower grid where different wire meshes can be placed to take into account the effect of the pore opening size on suffusion [13]. For this study, the opening size of the selected mesh screen is 4 mm to allow the migration of all fine particles and to reproduce in situ earth structures without filter, as a dike for example.

Seven specimens were prepared, three of them were placed in the oedopermeameter cell in three layers and each layer was compacted in order to reach

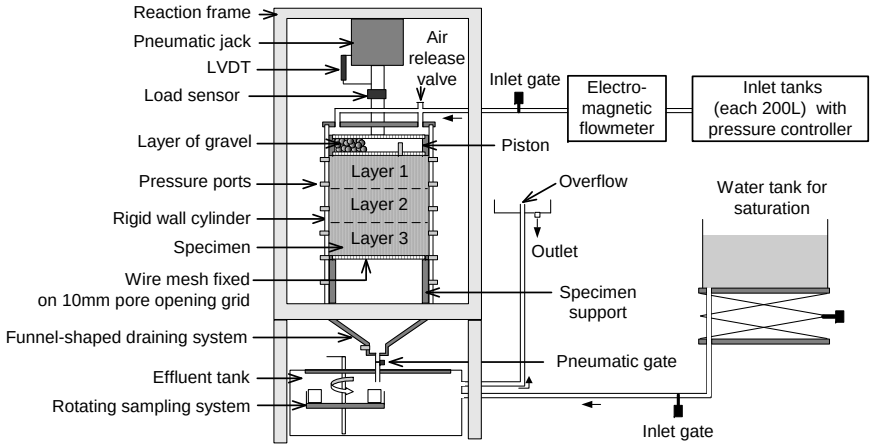

(a)

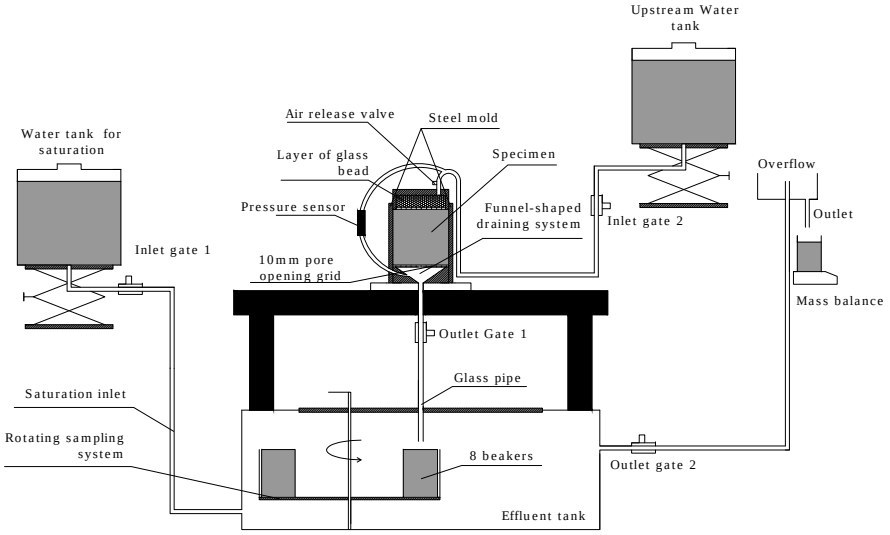

(b)

Fig. 1 Schematic diagram of (a) the oedopermeameter device and (b) the triaxial erodimeter device used in oedometric conditions.

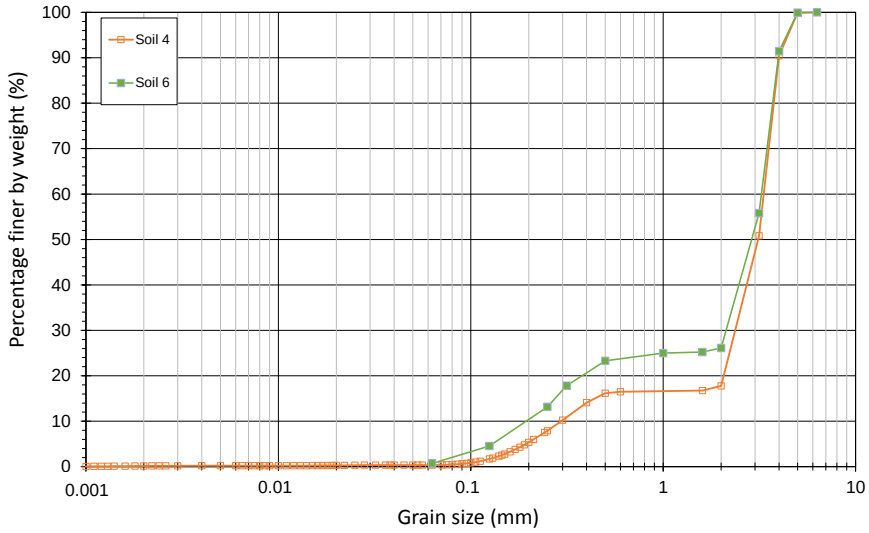

Fig. 2 Grain size distribution for the selected gap-graded soils (4) and (6).

the initial fixed dry density. Four specimens were prepared in the triaxial erodimeter device, using a single-layer semi-static compaction technique, in order to reach the target value of initial dry density. The upward saturation of all specimens started by injection of carbon dioxide to improve dissolution of gases into water, and finally, it was completed by adding water. Table 2 indicates the dry unit weight determined after the saturation phase for each specimen. A beaker was systematically used to catch the loss of particles during the saturation phase. Then, each specimen is subjected to a downward flow driven by a multistage hydraulic gradient as shown in Figures 3 and 4. A beaker was used to catch the eroded particles during each hydraulic gradient stage and the corresponding dry masses were measured. Table 3 details the eroded mass per unit volume measured at each stage of applied hydraulic gradient for all tested specimens.

Each test is characterized by its hydraulic conductivity whose computation is based on Darcy's formula. Some of the tests would incur a decrease of hydraulic conductivity whether at the first stages of the erosion process, 6-O-1, or during the whole erosion process, 4-T-1, 6-T-1 and 6-O-2 (see Figures 5 and 6). This decrease of hydraulic conductivity is attributed to some fine particles, detached and transported under the imposed water seepage and filtered within the soil itself. This filtration induces local clogging thus decreasing the hydraulic conductivity of the soil. The posterior increase in hydraulic conductivity, such as in the case of 6-O-1, is due to the washing out of fine particles

Table 2 Properties of tested specimens and summary of testing program

Specimen reference in paper	Specimen length (mm)	Initial dry density (kN/m^3)	Applied hydraulic gradient i $(-)$	Initial hydraulic conductivity $10^{-3}(m/s)$	Test duration (min)
4-O	437	15.87	From 0.04 to 0.16	37.83	167
4-T-1	50	16.08	From 0.10 to 1.50	0.64	153
4-T-2	100	16.12	From 0.04 to 0.71	0.47	170
6-O-1	430	17.31	From 0.04 to 0.50	3.54	181
6-O-2	435	16.74	From 0.04 to 0.77	5.64	310
6-T-1	50	16.96	From 0.09 to 7.50	0.03	252
6-T-3	100	16.95	From 0.09 to 1.13	1.08	157

Note on the specimen reference: The first number refers to the tested gradation and the last number is the specimen number; O = oedopermeameter; T = triaxial erodimeter.

Table 3 Applied hydraulic gradient and eroded mass per unit volume for all specimens

Specimen 4-O		Specimen 4-T-1		Specimen 4-T-2	
i_{av} (-)	$\bar{m}_{eroded}$ (kg/m^3)	i_{av} (-)	$\bar{m}_{eroded}$ (kg/m^3)	i_{av} (-)	$\bar{m}_{eroded}$ (kg/m^3)
0	5.845	0	4.176	0	0.713
0.039	2.561	0.004	4.584	0.002	0.051
0.064	3.029	0.1	0.102	0.073	0.051
0.092	5.742	0.2	0	0.104	0.204
0.123	7.443	0.3	0	0.137	0.025
0.133	2.877	1.4	0	0.289	0.051
				0.659	0.357

Specimen 6-O-1		Specimen 6-O-2		Specimen 6-T-1		Specimen 6-T-3	
i_{av} (-)	$\bar{m}_{eroded}$ (kg/m^3)	i_{av} (-)	$\bar{m}_{eroded}$ (kg/m^3)	i_{av} (-)	$\bar{m}_{eroded}$ (kg/m^3)	i_{av} (-)	$\bar{m}_{eroded}$ (kg/m^3)
0	7.254	0	11.203	0	3.259	0	5.297
0.035	3.359	0.044	0.562	0.004	0.102	0.019	0.102
0.094	0.208	0.089	0.191	0.199	0	0.036	0.153
0.191	1.342	0.135	0.532	0.397	0.306	0.045	0.255
0.295	6.287	0.177	1.139	0.759	0	0.198	0.407
0.411	29.468	0.273	5.068	1.736	0.102	0.445	0.611
0.563	25.737	0.432	7.18	2.707	0.051	1.078	4.074
		0.662	38.336	3.63	0.102		
				5.635	0.01		
				7.407	0.01		

Note: i_{av} is the average hydraulic gradient in a hydraulic step and $\bar{m}_{eroded}$ is the eroded mass collected from the initiation of each hydraulic step.

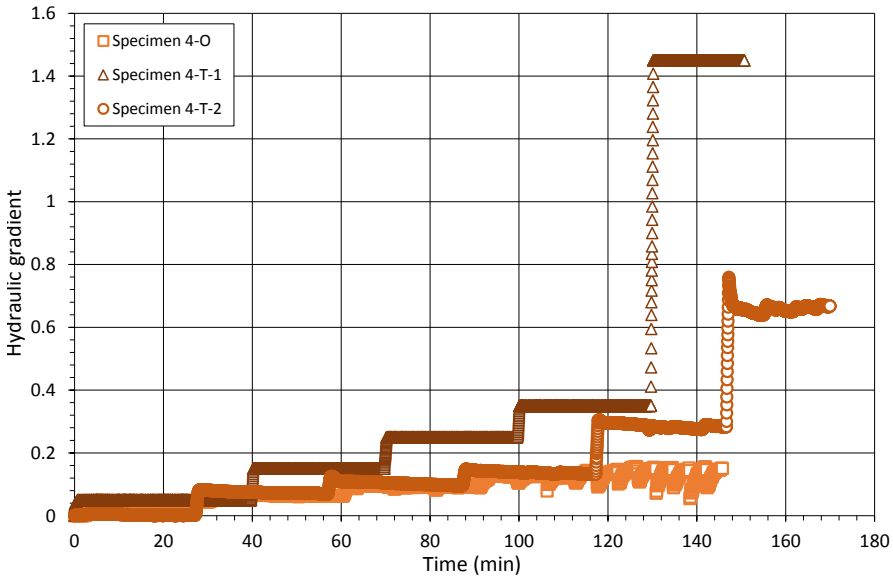

Fig. 3 Multi-stage hydraulic gradient conditions for the specimens of soil (4).

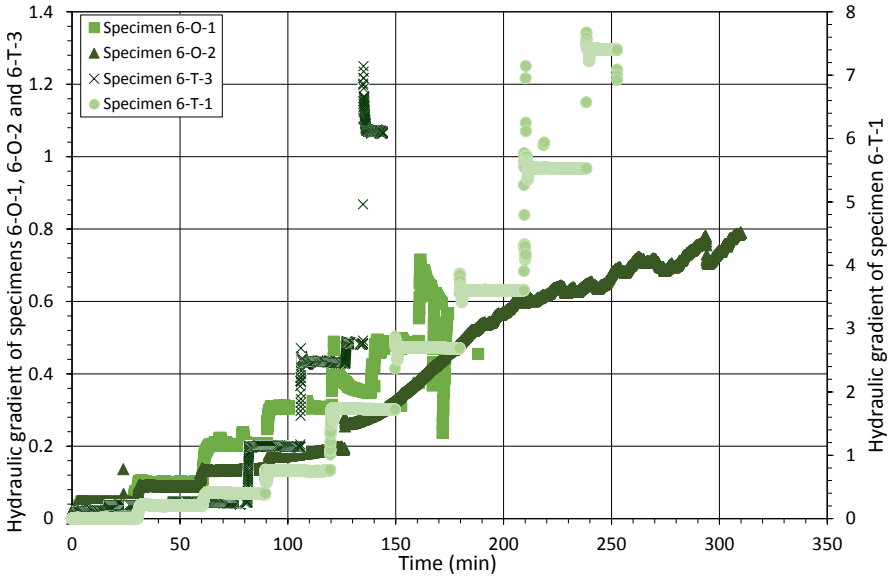

Fig. 4 Multi-stage hydraulic gradient conditions for the specimens of soil (6).

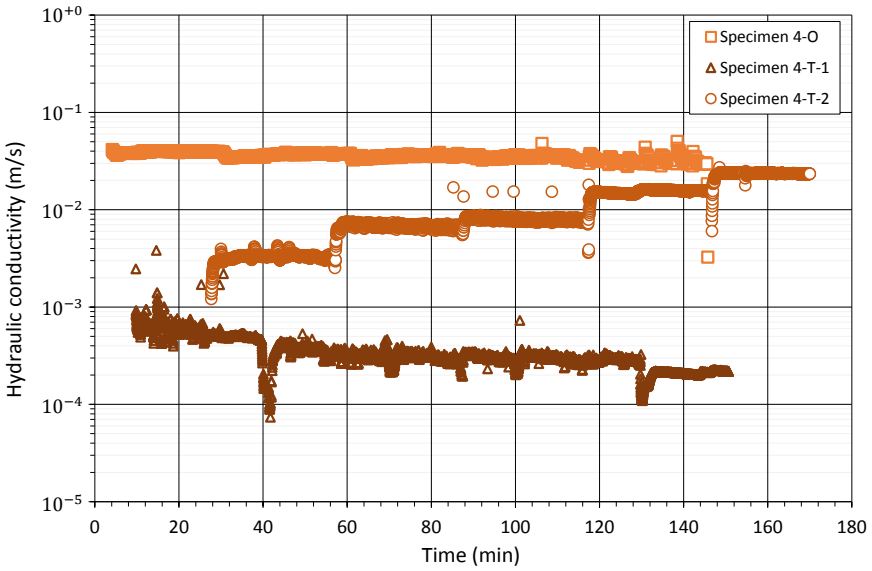

Fig. 5 Variation of the hydraulic conductivity of each specimen of soil (4) with time.

caused by much larger hydraulic gradients, overcoming the clogging aspect.

The cumulative eroded mass per unit volume of each specimen is displayed in Figures 7 and 8, for the seven tests. In a general manner, the eroded mass increases by steps [27], yet in our case the cumulated eroded mass for each step is displayed. This corresponds to the successive steps of the applied hydraulic gradient. These measured cumulative eroded masses form a reference to validate the ability of the proposed constitutive relationships to describe the kinetics of suffusion.

For a given particle size distribution, it is worth noting that the large discrepancy of the eroded dry mass per unit volume is due to the different initial dry densities of the specimens and the different histories of the applied hydraulic loading.

3 Describing the kinetics of suffusion

With the objective to reproduce the kinetics of the suffusion process, three constitutive relationships are compared. The first relationship is inspired from the hydraulic shear stress-based approach proposed by Reddi et al. [3] and usually used for modeling the development of hole erosion tests [23] or jet erosion tests [28]. The second relationship was proposed by Sibille et al. [24] for modeling suffusion tests by the mean of a power-based approach. Marot

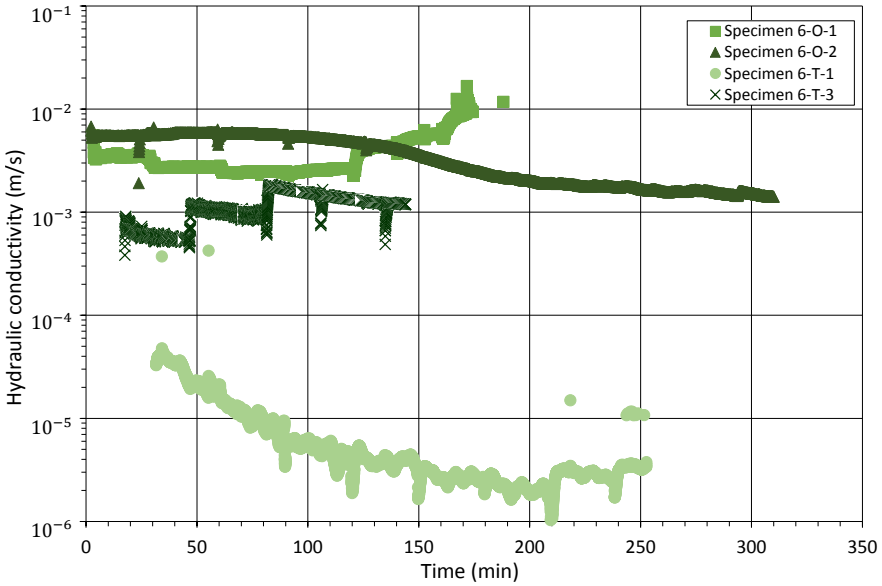

Fig. 6 Variation of the hydraulic conductivity of each specimen of soil (6) with time.

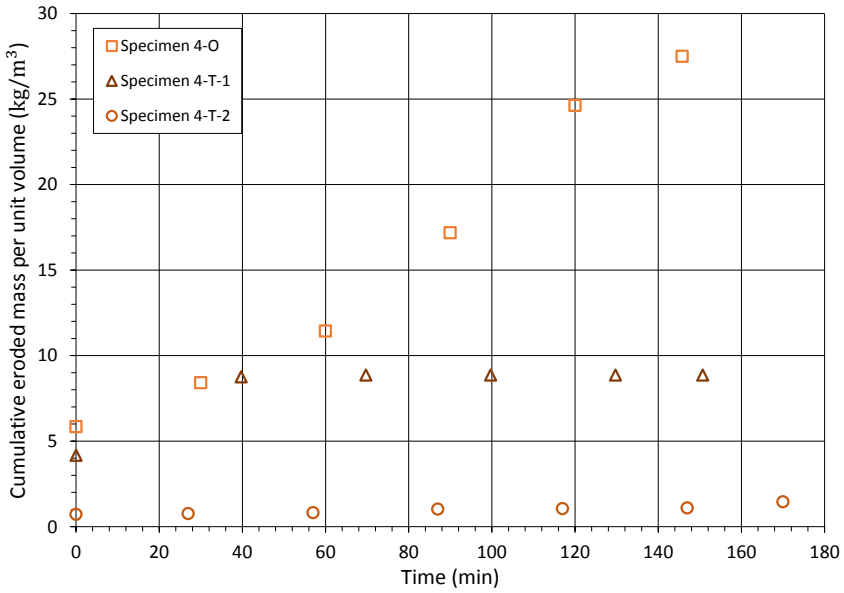

Fig. 7 Cumulative eroded mass per unit volume for the specimens of soil (4).

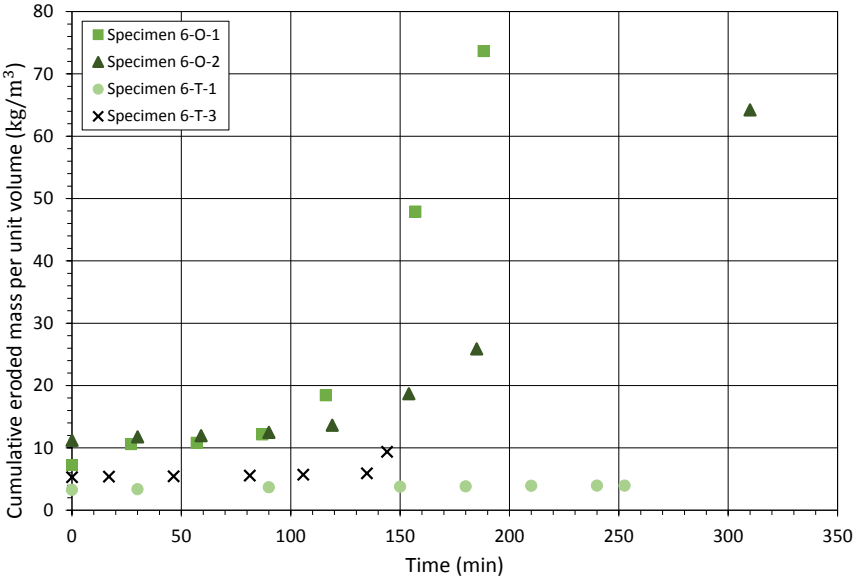

Fig. 8 Cumulative eroded mass per unit volume for the specimens of soil (6).

et al. [21] proposed the erosion resistance index in order to characterize the soil suffusion susceptibility. From this material property, a new energy-based constitutive relationship is developed.

3.1 The shear stress-based approach

A commonly used interpretative method for the hole erosion test [23] or the jet erosion test [28] consists of describing the erosion rate with a shear stress equation:

$$\dot{m} = Ce(\tau - \tau_c) \tag{5}$$

where $\dot{m}$ is the erosion rate per unit soil-water interface area and τ is the hydraulic shear stress, see eq. (1). This constitutive relationship linearly links the erosion rate with the hydraulic shear stress based on two parameters; Ce, which is the coefficient of erosion of the soil and τ_c, which is the critical hydraulic shear stress. It is worth highlighting that eq. (5) has been firstly developed for interface or concentrated leak erosion and for soil erodibility interpretations. Nevertheless, we wish to test its applicability to describe the development of suffusion.

To do so, the soil is modeled as a network of uniform-sized cylindrical capillary tubes, where the soil-water interface may be defined as the product of the average number of pores N_p by the average pore area S_p:

$$N_p = \frac{Sn^F}{\pi r_p^2} \quad ; \quad S_p = 2\pi r_p L \tag{6}$$

where S and L are the cross section and the length of the sample, respectively, n^F is the porosity and r_p is the average radius of pores defined by Garcia-Bengochea et al. [29] as a function of the intrinsic permeability k_F ,

$$r_p = \sqrt{\frac{8k_F}{n^F}} \tag{7}$$

Hence, $\dot{m}$ can be related to the erosion rate per unit volume (this volume is equal to the product of S and L) $\hat{\rho}^F$ by,

$$\dot{m} = \hat{\rho}^F \frac{1}{n^F} \sqrt{\frac{2k_F}{n^F}} \tag{8}$$

By means of eqs. (5) and (8), the following shear stress-based constitutive relationship is proposed,

$$\hat{\rho}^F = Ce(\tau - \tau_c) \frac{\sqrt{n^F} n^F}{\sqrt{2k_F}} \tag{9}$$

This shear stress-based equation or model uses two parameters: Ce and τ_c . The critical hydraulic shear stress τ_c is the shear stress corresponding to the minimum hydraulic load at which erosion is first initiated [23]. In other words, the critical hydraulic shear stress is physically related to a measurable initiation of suffusion. According to Skempton and Brogan [30], the onset of suffusion is characterized by an increase of hydraulic conductivity, thus the change of slope of the linear relation linking the flow velocity and the hydraulic gradient. The arrow sign in Figure 9 corresponds to the critical hydraulic gradient and hence the critical shear stress, at which suffusion initiates, for the soil specimen 6-O-1. However, a significant increase of slope is not always observed, so that the determination of the critical hydraulic gradient using such approach is not always possible, as for specimen 4-O in Figure 9. In such case, the critical hydraulic gradient is referred to the first applied hydraulic gradient.

The coefficient of erosion Ce is obtained from a linear approximation of the erosion rate $\dot{m}$ with respect to the hydraulic shear stress τ for $\tau > \tau_c$ (Figure 10). Yet, this linearity may not hold true up to the full suffusion state, see specimen 4-O in Figure 10. This is due to the fact that this coefficient was proposed by several researchers for interface or concentrated leak erosion where no clogging could interrupt the erosion process. On the other hand, suffusion may comprise some clogging which implies that the determination of Ce should be limited to the first suffusion phase only [15]. When a smooth linear relation characterized by a high coefficient of correlation R^2 between $\dot{m}$ and τ is not observed, only the beginning of the suffusion process is taken into account to identify, such as the case of specimen 4-O in Figure 10.

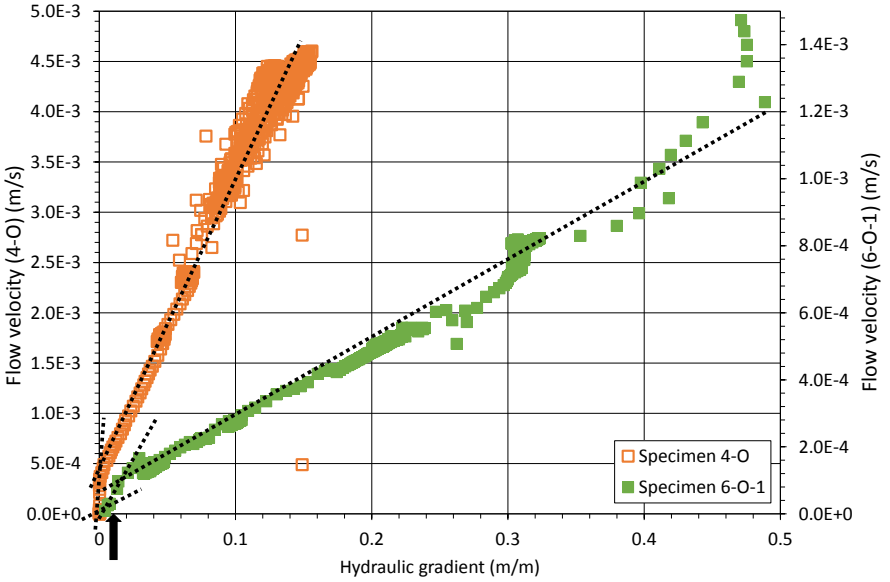

Fig. 9 Determination of the critical hydraulic gradient by the change of slope in the linear relation linking the flow velocity with the hydraulic gradient for the two specimens 4-O and 6-O-1, following Skempton and Brogan's approach [30].

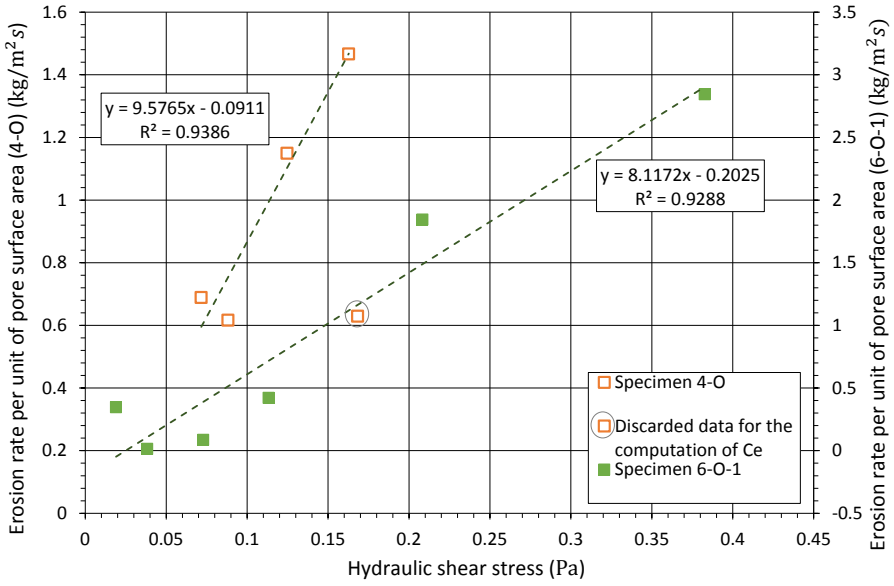

Fig. 10 Determination of the coefficient of erosion based on the linear relation linking the erosion rate per unit of pore surface area and the hydraulic shear stress for the two specimens 4-O and 6-O-1.

3.2 The power-based approach

A phenomenological model to describe the suffusion process has been proposed by Sibille et al. [24]. This model describes the erosion rate per unit volume of the eroded particles reaching the outlet of the specimen during a suffusion process $\hat{\rho}^F$ in terms of the instantaneous power expended by fluid flow, eq. (2), per unit volume denoted $\bar{P}_{flow}$,

$$\hat{\rho}^F = \alpha_{ref} \left[\frac{1}{\frac{\Delta \bar{E}_{stage}}{\bar{P}_{flow} t^*} + 1} \right] (\bar{P}_{flow})^{b_S} \tag{10}$$

where α_{ref} and b_S are parameters intrinsic to the material tested representing its erodibility, according to Sibille et al. [24], and t^* is a characteristic time relative to the tested material.

To take into account the history of the hydraulic loading, i.e. the amplitude and the duration of each stage, $\Delta \bar{E}_{stage}$, which is the flow energy per unit volume cumulated from the initiation of each hydraulic loading stage, is defined:

$$\Delta \bar{E}_{stage} = \int_{t_{init}}^{t>t_{init}} \bar{P}_{flow} dt \tag{11}$$

The power-based constitutive relationship (10) relies on three parameters, among which α_{ref} and b_S. Their determination is based on the characterization of the erosion rate at the initiation of each hydraulic loading step, as proposed by Sibille et al. [24]. This initiation is assumed to be representative of the detachment step, where the highest erosion rates can be observed. This is represented by the upper limit envelop of data approximated with the following power law,

$$\hat{\rho}^F_{upperlimit} = \alpha_{ref} (\bar{P}_{flow})^{b_S} \tag{12}$$

Nonetheless, detailed erosion rates on each hydraulic loading step could no longer be measured to favor a finer control of the downstream pressure (more frequent measurements would need closing and opening of the downstream valve which can produce harmful pressure surges). By adapting the power-based constitutive model to the data that we can actually measure, i.e. an averaged erosion rate for each hydraulic loading step, the same power law approximation, eq. (12), can be used to seek the parameters α_{ref} and b_S by means of the upper limit envelops plotted in Figures 11 and 12. Hence, we expect to slightly underestimate these parameters with respect to the original spirit of the model.

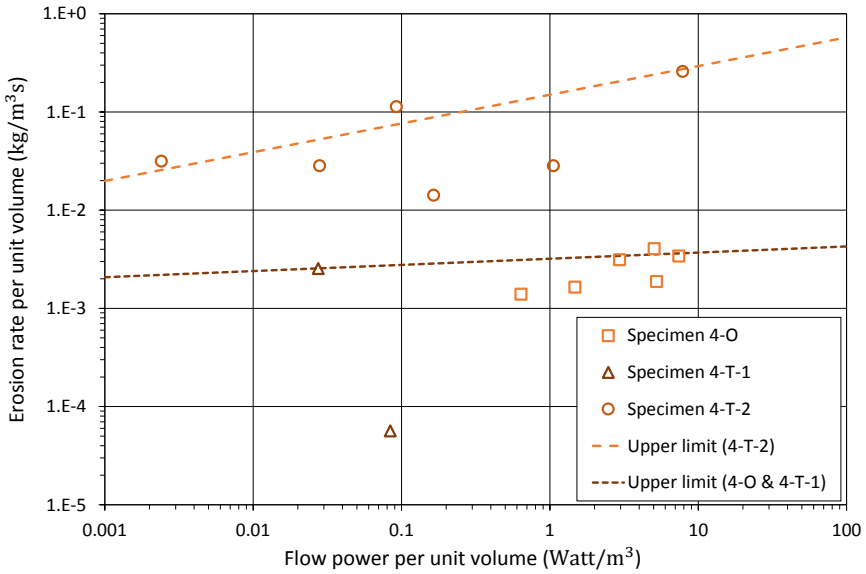

Fig. 11 Identification of the maximum erosion rate per unit volume as a function of the flow power per unit volume for the specimens of soil 4 using the upper limit envelop of the data.

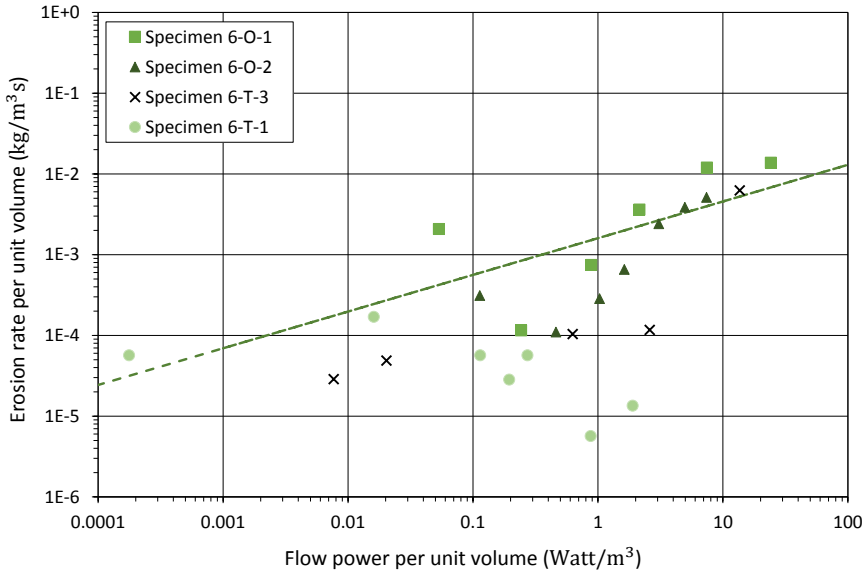

Fig. 12 Identification of the maximum erosion rate per unit volume as a function of the flow power per unit volume for the specimens of soil 6 using the upper limit envelop of the data.

3.3 The energy-based approach

The development of suffusion is studied by means of cumulative eroded mass collected at the outlet of the specimen. The cumulative eroded mass per unit volume $\bar{m}_{cum}(t)$ is plotted against the cumulative expended energy per unit volume $\bar{E}_{cum}(t)$, for both soils, in Figures 13 and 14. Both instantaneous cumulative quantities are defined by integrating over time the instantaneous volumetric eroded mass $\bar{m}_{eroded}$ and the instantaneous volumetric flow power $\bar{P}_{flow}$:

$$\bar{m}_{cum}(t) = \int_{t_0}^{t} \bar{m}_{eroded} dt \qquad \bar{E}_{cum}(t) = \int_{t_0}^{t} \bar{P}_{flow} dt \tag{13}$$

Throughout each suffusion test, the suffusion process is observed to reach a stable state of erodibility characterized by a constant permeability and a decreasing erosion rate [31]. This stable state is identified by the maximum cumulative eroded mass and the maximum cumulative expended energy. Actually, it is the point where the suffusion resistance index I_α (expressed by eq. (4)), as pointed out in Figures 13 and 14, can be defined,

$$\bar{m}_{max} = 10^{-I_\alpha} \bar{E}_{max} \tag{14}$$

where $\bar{m}_{max}$ and $\bar{E}_{max}$ are the maximum cumulative eroded mass and the maximum cumulative expended energy, respectively, per unit volume. Throughout, the overhead bar will refer to a volumetric quantity.

Based on this repeatable stable state of erodibility, eq. (14), we propose a dimensionless power relation linking the cumulative eroded mass and the cumulative expended energy, per unit volume,

$$\frac{\bar{m}_{cum}(t) - \bar{m}_{sat}}{\bar{m}_{max} - \bar{m}_{sat}} = \left(\frac{\bar{E}_{cum}(t)}{\bar{E}_{max}} \right)^{b(t)} \tag{15}$$

where $\bar{m}_{sat}$ is the mass lost during saturation phase per unit volume and $b(t)$ is a new parameter which controls the kinetics of suffusion. Small values of $b(t)$ indicate a fast kinetics and conversely. Aside from $\bar{m}_{sat}$ which is initially measured and from $b(t)$ which will be discussed below, the above constitutive relationship uses two parameters: the suffusion resistance index I_α by use of eq. (14) and the volumetric maximum cumulative expended energy $\bar{E}_{max}$; both parameters represent the erodibility of the material tested.

Since the erosion rate is expected to be large at the beginning of each loading step and to decrease during the step, $b(t)$ is expected to vary with time. By looking at eq. (15), the determination of $b(t)$ is limited by two restrictions: (i) $b(t)$ should be a dimensionless variable, and (ii) the cumulative eroded mass should never decrease to remain physically admissible. In that essence, $b(t)$ is defined as a function of the power dissipated by flow,

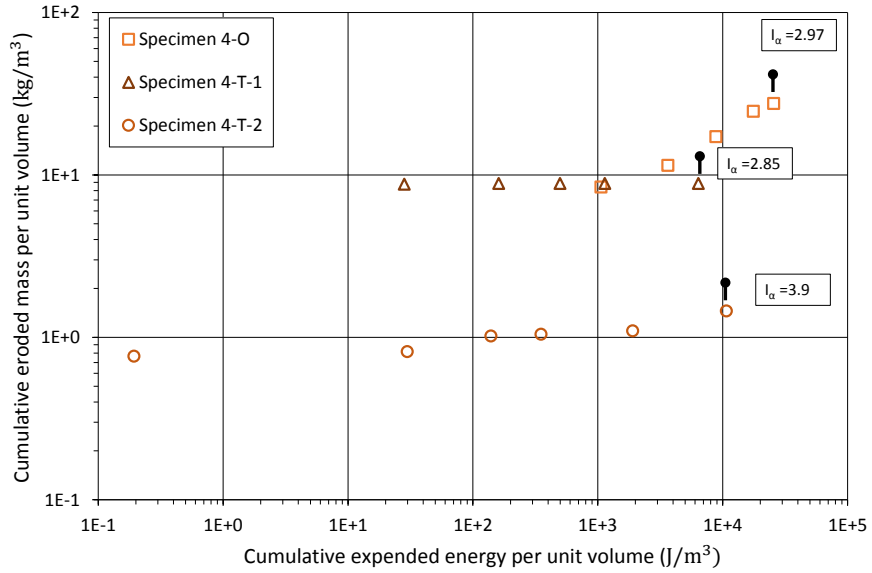

Fig. 13 Cumulative eroded mass per unit volume versus the cumulative expended energy per unit volume for the specimens of soil 4.

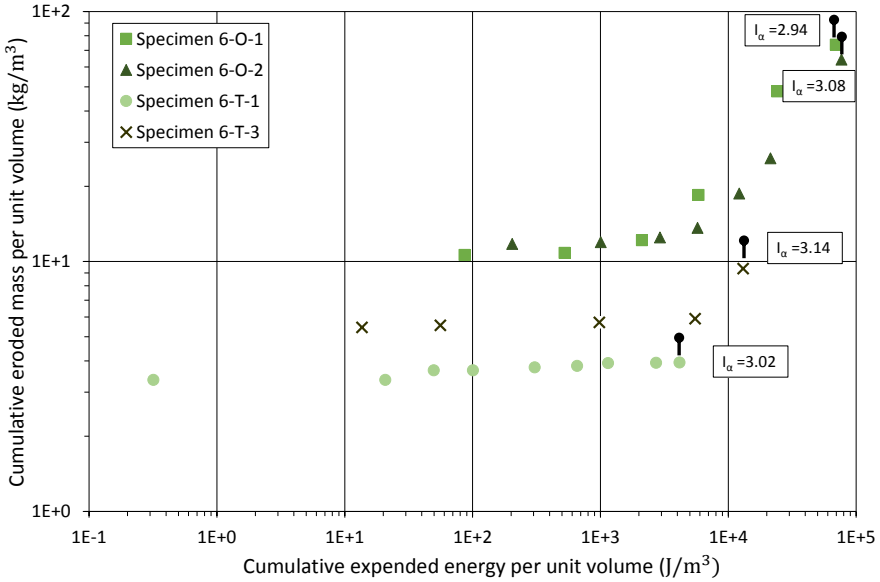

Fig. 14 Cumulative eroded mass per unit volume versus the cumulative expended energy per unit volume for the specimens of soil 6.

$$b(t) = \frac{P_{smoothed}(t)}{P_{flow}(t)} \tag{16}$$

where $P_{smoothed}(t)$ is the smoothed value of power determined based on a moving average method, under which the new smoothed values form a new series which is based on the averages of the original series [32], such as,

$$P_{smoothed}(t) = \text{mean}[P_{flow}(t) + P_{flow}(t-1) + P_{flow}(t-2) + \cdots + P_{flow}(t-n)] \tag{17}$$

where n corresponds to a number of instantaneous power values within a chosen smoothing time. In this study, the smoothing time is best fixed to 60 seconds and 10 seconds for soil 4 and 6, respectively. The influence of this smoothing time on the predicted eroded mass kinetics will be part of a future work.

4 Mass loss prediction with time

In order to validate the abilities of the energy-based proposed relationship eq. (15), the cumulative eroded mass is now compared with the cumulative eroded mass deduced from eqs. (9) and (10), where all are also compared with the collected mass measured during laboratory tests done by Le [25] and Zhong et al. [26]. The measured hydraulic conductivity (given in Figure 1) has been directly used for all the tests, and the constitutive relationship parameters are gathered in Table 4. A discussion on these parameters is provided in Section 5.

For the different examined specimens, the three suffusion constitutive relationships are able to capture the beginning of suffusion process, as shown in Figure 15. However, the prediction of the eroded mass using the shear stress-based constitutive relationship is not totally in agreement with the experimental data. This shear stress-based model predicts linearly the kinetics of suffusion, due to the linear relation defined, originally, between the erosion rate per unit of volume and the hydraulic shear stress, as highlighted in eq. (9). Concerning specimens 4-O and 6-T-3, the cumulative eroded mass predicted using this model agrees well with the experimental results during the progress of the suffusion process, though it overestimates the end of the test for the former and it underestimates the end for the latter. Concerning specimens 4-T-1, 4-T-2, 6-T-1, 6-O-1 and 6-O-2, a discrepancy, ranging from being large for the first three specimens to being moderate for the last two, can be observed between the predicted values using the shear stress-based constitutive relationship and the experimental results, upon the progress of the suffusion process. The gap between the predicted values and the experimental results is attributed to the lack of linearity between the erosion rate per unit of volume and the hydraulic shear stress. In fact, some specimens experience a decrease of erosion rate with time, reflected by a constant cumulative eroded

mass, for example specimens 4-T-1 and 4-T-2. As a consequence, it is difficult for the linear smooth relation to represent the whole suffusion process. For all specimens, except 6-O-1 and 6-O-2, the linear relation linking the erosion rate per unit of pore surface area and the hydraulic shear stress, is only valid at the beginning of the suffusion test. Thus, the progress of the suffusion process becomes out of control of this constitutive relationship. This result is in agreement with Reddi et al. [3]'s finding that the fate of eroded particles including redeposition and pore clogging may govern the internal erosion process far more than the surface erodibility.

The correspondence between the cumulative eroded mass predicted using the power-based constitutive relationship and the experimental results is very good for specimens 4-O, 4-T-2, 6-T-1 and 6-T-3, and qualitatively good for 4-T-1. The cumulative eroded mass is predicted in a step-like evolution which is a mimic of the real experimental evolution of the eroded mass during suffusion process. This step-like evolution can be attributed to the $\Delta \bar{E}_{stage}$ parameter which takes into account the history of the hydraulic loading for each hydraulic step, see eq. (10). For specimens 6-O-1 and 6-O-2, the cumulative eroded mass is predicted linearly asymptotic slightly below or above the experimental results. This discrepancy can be related to the parameters and that might have been underestimated due to the use of an averaged erosion rate for each hydraulic loading step rather than a more detailed erosion rate (Figures 11 and 12). At variance with the work of Sibille et al. [24], the characteristic time is best fitted for each specimen. A discussion on these values is later provided in Section 5.

Concerning the cumulative eroded mass predicted using the energy-based constitutive relationship, it is able to capture fairly well the step-like evolution, characteristic of a suffusion behavior, for all the specimens. This estimation is able to describe, in a qualitative manner, the evolution of the suffusion process for most of the cases. Indeed, the quite good agreement between the simulated results and the experimental ones is assigned to the adoption of the energy-based approach of Marot et al. [31], under which the hydraulic loading is best represented by the power dissipated by flow. Moreover, this constitutive relationship sheds light on the final state of suffusion, by which the end of suffusion process is relied upon. By taking into account both the hydraulic loading and the soil response, the energy-based relationship parameter $b(t)$ has made it possible to represent the suffusion evolution in a quite valuable manner. However, the prediction of eroded mass is not totally in agreement with the experimental data. This imperfection may be related to the $b(t)$ parameter that is defined based on two hypotheses: (i) the suffusion kinetics is solely related to the evolution of the power dissipated by the flow P_{flow}, see eq. (16), and (ii) the suffusion evolution is arbitrarily influenced by its recent history (10 and 60 seconds) through the parameter . The discrepancies between the prediction and the experimental data raise the need for further

investigations on the kinetics parameter and on the influence of the smoothing time.

5 Implications for modeling purposes

Although the above constitutive relationships have not been obtained within the framework of thermodynamics of irreversible processes [33] [34], they represent to date the only means of describing the suffusion process. The stakeholder needs in terms of risk management of embankment structures urge researchers to model suffusion at a structure scale [35]. This urge requires to verify the parameters accuracy and their relation with the seepage length.

Table 4 exhibits all the parameters for each specimen. Parameters intrinsic to a tested material should not be influenced by the seepage length but can be influenced by the initial micro-structure. For example, denser specimens should be less erodible than looser specimens [36]. Therefore, the deviation from the mean of the ratio of several parameters to the corresponding dry unit weight is compared against the seepage length, as illustrated in Figure 16. If the mean is assumed to represent the exact value, this result may be viewed as a relative error.

The first parameter to be discussed is the coefficient of erosion Ce. As mentioned previously, the shear stress-based constitutive relationship is inspired from the concentrated leak /interface erosion model proposed by Wan and Fell [23]. The authors found that the coefficient of erosion is strongly influenced by the degree of compaction and the water content, hence the degree of saturation at compaction of the soil. Moreover, this parameter was found to be inversely proportional to the unit dry density of the specimen. The erodibility indeed depends on inter-particles forces, mainly of physical-chemical nature for clayey soil and interlocking for cohesionless soils. Yet, these forces depend on the average distance between particles which decreases with the dry density growth. Figure 16 reveals that the coefficient of erosion $Ce \times \gamma_d$ is characterised by a noticeable dispersion of its relative error with the flow length. This result suggests that Ce is not an intrinsic parameter.

Concerning the critical hydraulic shear stress τ_c, Table 4 shows that for different specimens of the same soil, the values of τ_c are considerably different. This reflects that there is a large degree of inaccuracy in the estimation of τ_c. This is in agreement with the findings of Wan and Fell [23] in what concerns this parameter. As a sequel, the influence of the spatial scale on this parameter cannot be studied accurately.

The second point of discussion deals with the parameters of the power-based constitutive relationship. In a general manner, the two parameters α_{ref} and b_S are intrinsic to the material and represent its erodibility [24]. This

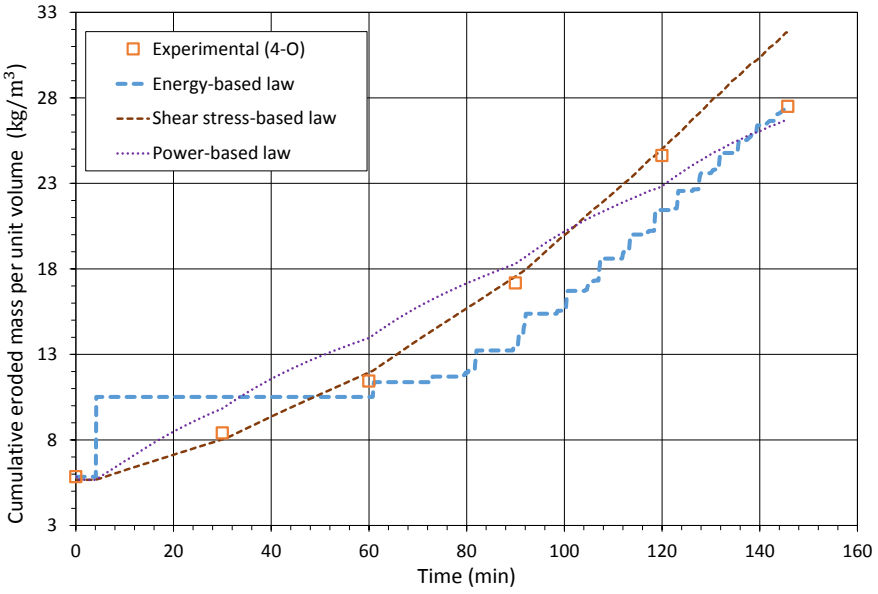
Experimental (4-O)
Energy-based law
Shear stress-based law
Power-based law
Cumulative eroded mass per unit volume (kg/m3)
Time (min)
33
28
23
18
13
8
3
0
20
40
60
80
100
120
140
160

(a)

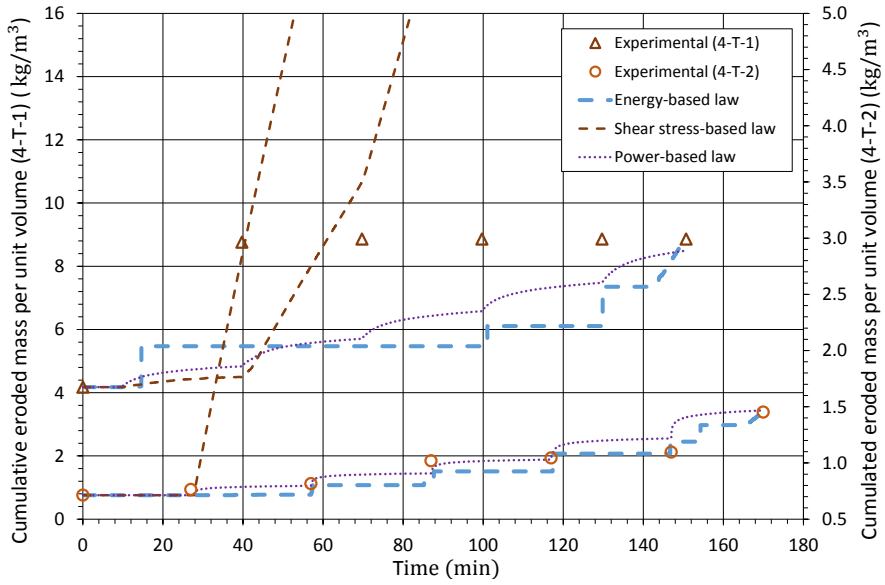
Experimental (4-T-1)
Experimental (4-T-2)
Energy-based law
Shear stress-based law
Power-based law
Cumulative eroded mass per unit volume (4-T-1) (kg/m3)
Cumulated eroded mass per unit volume (4-T-2) (kg/m3)
Time (min)
16
14
12
10
8
6
4
2
0
5.0
4.5
4.0
3.5
3.0
2.5
2.0
1.5
1.0
0.5
0
20
40
60
80
100
120
140
160
180

(b)

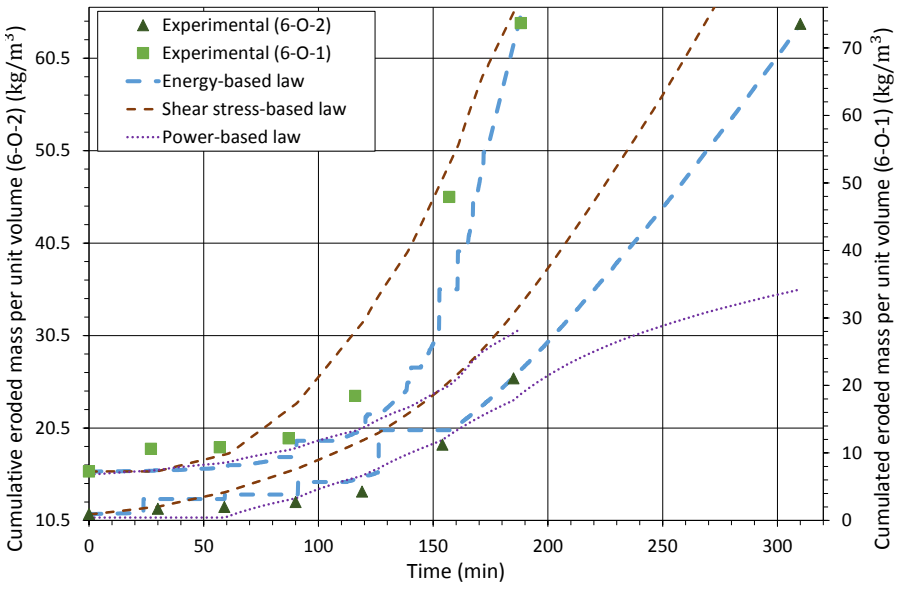

(c)

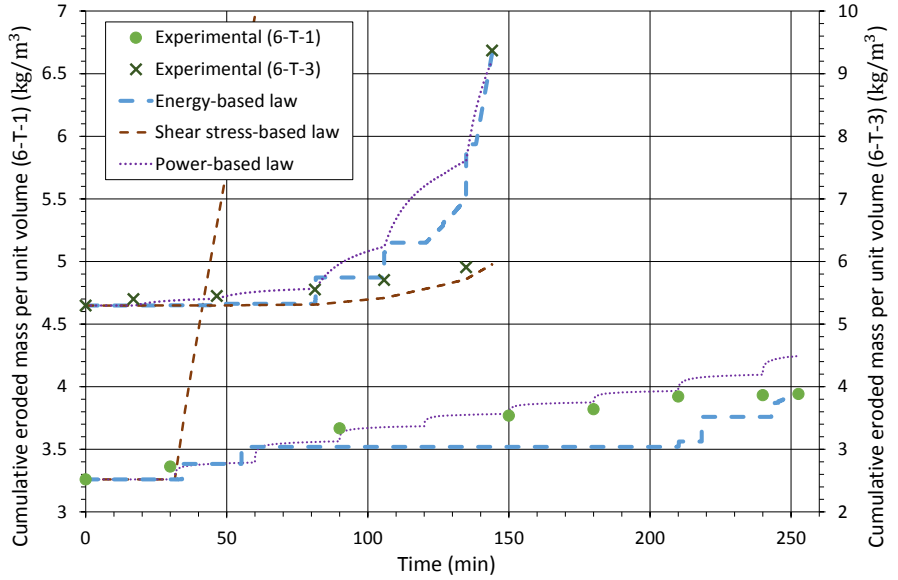

(d)

Fig. 15 Comparison of the cumulative eroded mass predicted using the shear stress-based constitutive relationship, the energy-based constitutive relationship, and the power-based constitutive relationship with the collected mass measured during laboratory tests for (a) specimen 4-O, (b) specimens 4-T-1 and 4-T-2, (c) specimens 6-O-1 and 6-O-2, and (d) specimens 6-T-1 and 6-T-3.

intrinsic character is reflected in those parameters corresponding to the specimens of soil 6, see Table 4. Nonetheless, it is not the case for specimens of soil 4, due to the adaptation of the power-based model to the data that we can actually measure. On the other hand, t^* was initially defined as a characteristic time relative to the tested material [24], yet Figure 16 suggests otherwise. It shows that the characteristic time is highly affected by the spatial scale due to the noticeable dispersion of the corresponding relative error.

Finally, the erosion resistance index I_α used within the energy-based constitutive relationship is tackled. This parameter is the core of the energy-based constitutive relationship. It corresponds to the end of the suffusion process (Figures 13 and 14) and relates the maximum cumulative eroded mass with the maximum cumulative dissipated energy. Zhong et al. [26] have demonstrated that, the dissipated energy and the eroded mass depend on the size of the specimen; thus, the resistance index which is the ratio of these two quantities is independent of the specimen size. This is validated by Figure 16 which shows that the maximum relative error of I_α/γ_d is 18%, ensuring that I_α is fairly independent with respect to the flow length and seems to be an intrinsic parameter for a soil, at least at the laboratory scale.

The other parameter that is required by the energy-based constitutive relationship is the volumetric maximum cumulative dissipated energy $\bar{E}_{max}$. As mentioned previously, this parameter is related to the maximum cumulative eroded mass as a function of the erosion resistance index I_α. According to Zhong et al. [26], this parameter varies with the size of the specimen, which is validated in Figure 17. This figure shows that $\bar{E}_{max}/\gamma_d$ seems to increase with the flow length for both tested soils, highlighting that $\bar{E}_{max}$ is probably proportional to the seepage length. Indeed, the maximum volumetric cumulated energy $\bar{E}_{max}$ dissipated by suffusion involves three mechanisms: detachment, transport and possible filtration of the fines particles. While the volumetric energy used for the detachment should not be influenced by the flow length, it is expected that more volumetric energy will be dissipated for the transportation of fines particles through a porous medium when the seepage length increases. The same is expected for the filtration mechanisms. This proportionality tendency between $\bar{E}_{max}/\gamma_d$ and the flow length will be broaden to other soils and other flow lengths as a future work.

In terms of modeling implication, the use of the power-based approach is complicated by the history term $\Delta\bar{E}_{max}$ because its computation requires the knowledge of the beginning and the end of each loading step. Although this knowledge is fairly obvious for laboratory specimens tested under multi-stage hydraulic gradient conditions, it can become unclear when considering hydraulic loading conditions in the field. This observation is at the root of the development of the energy-based constitutive relationship eq. (14).

Table 4 Constitutive parameters for each specimen

Parameter		Specimen						
		4-O	4-T-1	4-T-2	6-O-1	6-O-2	6-T-1	6-T-3
I_α	(s^2/m^2)	2.97	2.85	3.9	2.97	3.08	3.02	3.14
$\bar{E}_{max}$	$10^3(J/m^3)$	25.646	6.378	10.723	69.403	76.782	4.161	13.058
Ce	$10^{-6}(s/m)$	9.5	10.33	10.4	8.11	2.86	4.02	0.119
τ_c	$10^{-3}(Pa)$	0	7.7	0.7	18.99	0	1.84	6.6
α_{ref}	$10^{-2}(s^2/m^2)$	0.32	0.32	11.95	0.16	0.16	0.16	0.16
b_S	$10^{-2}(-)$	7.1	7.1	19.525	45.45	45.45	45.45	45.45
t^*	(s)	1800	100	0.2	1800	1800	10	280

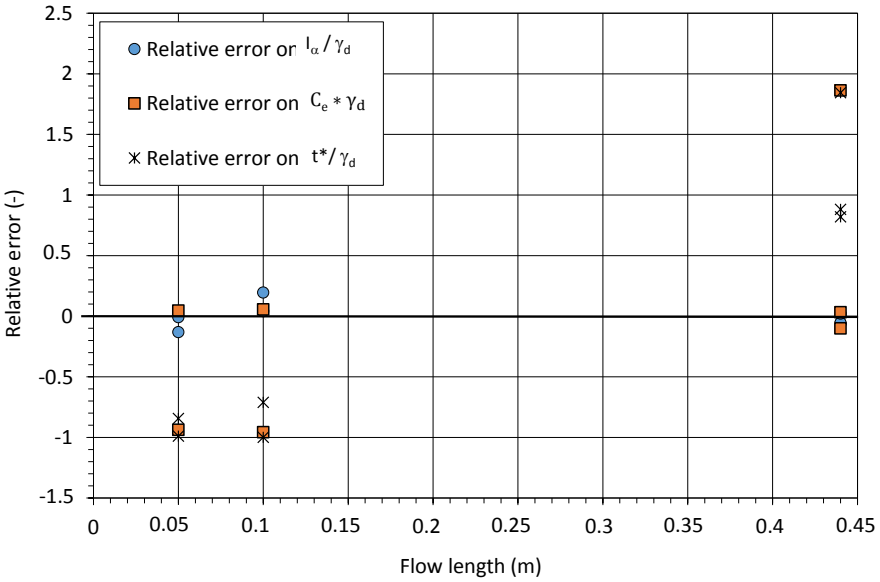

Fig. 16 The variation of the relative error of: the erosion resistance index I_α , the coefficient of erosion Ce, and the characteristic time t^* with the flow length.

The description proposed is able to capture the main features of the erosion process for various specimen sizes and hydraulic loading histories. In addition, the cornerstone of this description, i.e. the parameter I_α seems to be independent of the spatial scale, at least at the laboratory scale [26,15]. However, the prediction proposed is not totally in agreement with the experimental data. These differences could be attributed to the smoothing time value. These considerations raise the need for additional investigations to better understand the influence of this smoothing time and its physical meaning.

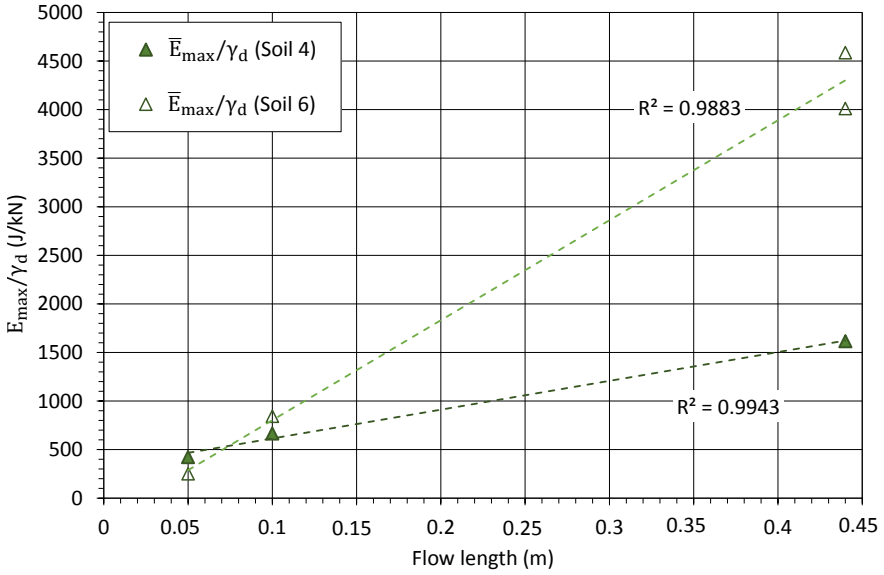

Fig. 17 The variation of the ratio of the maximum cumulative dissipated energy with respect to the dry unit weight $\bar{E}_{max}/\gamma_d$ with the flow length.

6 Conclusion

In this paper, a new suffusion constitutive relationship, inspired from the energy-based approach is proposed. This relationship is compared against two other constitutive relationships inspired from literature. The first is the shear stress-based model initially developed for interface/concentrated leak erosion and adapted to suffusion. The second is the power-based constitutive relationship proposed for the suffusion process, but adapted to the data that we can actually measure.

The proposed energy-based constitutive relationship is able to imitate quite well the experimental results for all specimens. On the other hand, despite the fact that the power-based constitutive relationship is able to predict quite well the step-like evolution of the eroded mass for some specimens, it misses this evolution for other specimens by providing a linear asymptotic prediction or an under-estimated prediction. Concerning the shear stress-based constitutive relationship, it appears relatively inappropriate to represent the kinetics of suffusion. While in some cases this prediction is not totally in agreement with the experimental results, in most cases it cannot grasp the development of the suffusion process.

Moreover, the intrinsic characteristic of the parameters of each constitutive relationship is discussed. Starting with the shear stress-based relationship, the

coefficient of erosion Ce is characterized by a large relative error and the critical hydraulic shear stress τ_c could not be accurately measured. On the other hand, the parameters of the power-based relationship, α_{ref} and b_S, are found to be intrinsic for one soil and not for the other, and the characteristic time t^* displays a large relative error. Finally, the erosion resistance index I_α used within the energy-based relationship is validated as intrinsic parameter, at least at the laboratory scale, while the volumetric maximum cumulated energy $\bar{E}_{max}$ seems, as expected, to increase with the flow length. When considering modeling implications, the power-based proposition seems more constrained than the energy-based model due to its history parameter $\Delta\bar{E}_{stage}$. The validation of the new erosion constitutive relationship at the structure scale will require the simulation of real earth structures, but unfortunately, available data are scarce. Such simulation will be addressed in a future work.

Acknowledgements The authors would like to acknowledge the National Council for Scientific Research of Lebanon (CNRS-L) and the Lebanese University (UL) for providing a financial support for this work.

References

1. Foster M, Fell R, Spannagle M (2000) The statistics of embankment dam failures and accidents. Canadian Geotechnical Journal 37(5):1000–1024
2. Fell R, Fry JJ (2014) The state of the art of assessing the likelihood of internal erosion of embankment dams, water retaining structures and their foundations. In: Internal Erosion of Dams and Their Foundations, Aussois, France, 25–27 April 2005, CRC Press, pp 9–32
3. Reddi LN, Lee IM, Bonala MV (2000) Comparison of internal and surface erosion using flow pump tests on a sand-kaolinite mixture. Geotechnical testing journal pp 116–122
4. Bendahmane F, Marot D, Alexis A (2008) Experimental parametric study of suffusion and backward erosion. Journal of Geotechnical and Geoenvironmental Engineering pp 57–67
5. Marot D, Benamar A (2012) Suffusion, transport and filtration of fine particles in granular soil. S. Bonelli, Éd., London, ISTE
6. Horikoshi K, Takahashi A (2015) Suffusion-induced change in spatial distribution of fine fractions in embankment subjected to seepage flow. Soils and Foundations 55(5):12931304
7. Nguyen CD, Benahmed N, Andó E, Sibille L, Philippe P (2019) Experimental investigation of microstructural changes in soils eroded by suffusion using x-ray tomography. Acta Geotechnica 14(3):749765
8. Hu Z, Yida Z, and Zhongxuan Y (2019) Suffusion-induced deformation and microstructural change of granular soils: a coupled CFD-DEM study. Acta Geotechnica 14.3: 795-814.
9. Yang J, Yin ZY, Laouafa F, Hicher PY (2019) Modeling coupled erosion and filtration of fine particles in granular media. Acta Geotechnica 14(6):16151627
10. Moffat RA, Fannin RJ (2006) A large permeameter for study of internal stability in cohesionless soils. Geotechnical Testing Journal 29(4):273279
11. Sail Y, Marot D, Sibille L, Alexis A (2011) Suffusion tests on cohesionless granular matter: Experimental study. European Journal of Environmental and Civil Engineering 15(5):799–817
12. Nguyen CD (2018) Etude expérimentale de limpact de lérosion par suffusion sur les propriétés physiques et mécaniques des sols. PhD thesis, Aix-Marseille
13. Marot D, Bendahmane F, Rosquoet F, Alexis A (2009) Internal flow effects on isotropic confined sand-clay mixtures. Soil & Sediment Contamination 18(3):294306

14. Nguyen HH, Marot D, Bendahmane F (2012) Erodibility characterisation for suffusion process in cohesive soil by two types of hydraulic loading. La Houille Blanche (6):5460
15. Rochim A, Marot D, Sibille L, Thao Le V (2017) Effects of hydraulic loading history on suffusion susceptibility of cohesionless soils. Journal of Geotechnical and Environmental Engineering 143(7)
16. Chang DS, Zhang LM (2013) Extended internal stability criteria for soils under seepage. Soils and Foundations 53(4):569583
17. Kenney T, Lau D (1985) Internal stability of granular filters. Canadian geotechnical journal 22(2):215225
18. Reboul N, Vincens E, Cambou B (2010) A computational procedure to assess the distribution of constriction sizes for an assembly of spheres. Computers and Geotechnics 37(1-2):195206
19. Kovacs G (1981) Developments in water science seepage hydraulics, chap 3.2
20. Marot D, Le VD, Garnier J, Thorel L, Audrain P (2012) Study of scale effect in an internal erosion mechanism: centrifuge model and energy analysis. European Journal of Environmental and Civil Engineering 16(1):1–19
21. Marot D, Rochim A, Nguyen HH, Bendahmane F, Sibille L (2016) Assessing the susceptibility of gap-graded soils to internal erosion: proposition of a new experimental methodology. Natural Hazards 83(1):365388
22. Vardoulakis I, Papamichos E (1991) Surface instabilities in elastic anisotropic media with surface-parallel griffith cracks. In: International Journal of Rock Mechanics and Mining Sciences & Geomechanics Abstracts, Elsevier, vol 28, pp 163–173
23. Wan CF, Fell R (2004) Investigation of rate of erosion of soils in embankment dams. Journal of geotechnical and geoenvironmental engineering 130(4):373–380
24. Sibille L, Marot D, Sail Y (2015) A description of internal erosion by suffusion and induced settlements on cohesionless granular matter. Acta geotechnica 10(6):735–748
25. Le VT (2017) Development of a new device and statistical analysis for characterizing soil sensibility face suffusion process. PhD thesis, Université de Nantes
26. Zhong C, Le VT, Bendahmane F, Marot D, Yin ZY (2018) Investigation of spatial scale effects on suffusion susceptibility. Journal of Geotechnical and Geoenvironmental Engineering 144(9):04018067
27. Chang D, Zhang L (2011) A stress-controlled erosion apparatus for studying internal erosion in soils. Geotechnical Testing Journal 34(6):579–589
28. Hanson G, Simon A (2001) Erodibility of cohesive streambeds in the loess area of the midwestern USA. Hydrological processes 15(1):23–38
29. Garcia-Bengochea I, Altschaeffl AG, Lovell CW (1979) Pore distribution and permeability of silty clays. Journal of the Geotechnical Engineering Division 105(7):839–856
30. Skempton A, Brogan J (1994) Experiments on piping in sandy gravels. Geotechnique 44(3):449–460
31. Marot D, Regazzoni PL, Wahl T (2011) Energy-based method for providing soil surface erodibility rankings. Journal of Geotechnical and Geoenvironmental Engineering 137(12):1290–1293
32. Hyndman RJ, Athanasopoulos G (2018) Forecasting: principles and practice. OTexts
33. Bui TA, Gelet R, Marot D (2019) Modelling of internal erosion based on mixture theory: General framework and a case study of soil suffusion. International Journal for Numerical and Analytical Methods in Geomechanics 43(15):24072430
34. Rousseau Q, Sciarra G, Gelet R, Marot D (2020) Modelling the poroelastoplastic behaviour of soils subjected to internal erosion by suffusion. International Journal for Numerical and Analytical Methods in Geomechanics 44(1):117136
35. Zhang X, Wong H, Leo CJ, Bui TA, Wang J, Sun W, Huang Z (2013) A thermodynamics-based model on the internal erosion of earth structures. Geotechnical and Geological Engineering 31(2):479–492
36. Le V, Marot D, Rochim A, Bendahmane F, Nguyen H (2016) Suffusion susceptibility characterization by triaxial erodimeter and statistical analysis. In: Scour and Erosion: Proceedings of the 8th International Conference on Scour and Erosion (Oxford, UK, 12-15 September 2016), CRC Press, p 453